# A Nonlinear Observer Approach of SOC Estimation Based on Hysteresis Model for Lithium-ion Battery

Yan Ma, Bingsi Li, Guangyuan Li, Jixing Zhang, and Hong Chen, *Senior Member, IEEE*

***Abstract*—In this paper, a state of charge (SOC) estimation approach for lithium-ion battery based on equivalent circuit model and the input-to-state stability (ISS) theory has been proposed. According to the electrochemical performance of lithium-ion battery, the equivalent circuit model with two RC networks is established, which includes hysteresis characteristic in inner electrochemical response process. The nonlinear relation between open circuit voltage (OCV) and SOC is obtained from a rapid test. Exponential fitting method is used to identify the parameters of the model. A novel state observer based on ISS theory is designed for lithium-ion battery SOC estimation. The designed observer is tested on AMESim and Simulink co-simulation. The simulation results show that the proposed method has a high SOC estimation accuracy with an error of about 2 percent.**

***Index Terms*—AMESim, hysteresis model, input-to-state stability (ISS) observer, Lithium-ion battery, state of charge (SOC).**

## I. Introduction

LITHIUM-ION batteries have high levels of energy and power density among electrochemical batteries. These attributes make them suitable to be the energy storage system in electric vehicle, hybrid electric vehicle, and plug-in hybrid electric vehicle (EV/HEV/PHEV) [1]. One of the important requirements in automotive batteries is to monitor their real time state of charge (SOC). SOC of the battery is not readily available during charging and discharging cycles. SOC values have to be predicted based on the measured terminal voltage and current [2].

SOC reflects the remaining capacity that can be drawn from the battery pack and is used to ensure an optimum control of charging and discharging processes. However, several factors of SOC determination for batteries such as hysteresis phenomena, flat characteristic of open circuit voltage (OCV) over SOC, and limited voltage measurement accuracy can result in SOC estimation error [3].

In recent years, great effort has been exercised to improve the accuracy of SOC estimation. There are two main kinds of methods for SOC estimation at present. One is calculating SOC by charge-discharge current and OCV based on energy conservation and inner physical characteristics of the lithium-ion cell. The classical approach of current integration (Coulomb counting) which samples the battery current and computes the accumulated charge and discharge to estimate SOC, is simple and inexpensive to implement, but it cannot solve the problems of accumulative error and inaccurate initial values. Open circuit voltage commonly needs relatively long rest periods in applications. Since the rest periods will only occur from time to time, the open circuit voltage measurement is usually combined with other techniques [4]. Other methods, such as discharge test or internal resistance characteristic, are usually considered as laboratory methods. The obvious disadvantages of non-model based estimation methods are the limited accuracy, long estimation time and only offline application in spite of the advantages as simple principle and easy implementation [5].

The other is indirectly estimating SOC based on the mathematical model of the lithium-ion cell. State estimation with Luenberger observer has already been analyzed [6]. Kalman filter (KF) approach with its knowledge about statistical characteristics of process and measurement noise is intensively studied. Extended Kalman filter (EKF) and sigma point Kalman filter (SPKF) are two improvements to the classical KF which are investigated for nonlinear systems [7]−[9]. The support vector machine (SVM) and sliding mode observer (SMO) can simulate the complicated battery dynamics, but the performance of these techniques is sensitive to training data. Therefore, it is not appropriate for the battery online application [10], [11].

The well-known input-to-state stability (ISS) property of deterministic systems originated in [12] and was investigated quite intensively in recent years [13], [14]. Especially, some concepts of ISS observer have appeared in [15]. Considering the parameter uncertainties and the unmodeled dynamics as disturbance inputs [16], analyzed the robust stability of the closed loop estimation error system based on the ISS theory, and gave estimation system parameter adjustment guidelines on this basis.

It is obvious that proper design, engineering and operation

Manuscript received October 31, 2015; Accepted April 1, 2016. This work was supported by the High Technology Research and Development Program of Jilin (20130204021GX), the Specialized Research Fund for Graduate Course Identification System Program (Jilin University) of China (450060523183), the National Natural Science Foundation of China (61520106008, U1564207, 61503149), the Education Department of Jilin Province of China (2016430), and the Graduate Innovation Fund of Jilin University (2016030). Recommended by Associate Editor Xiangyang Zhao.

Citation: Y. Ma, B. S. Li, G. Y. Li, J. X. Zhang, and H. Chen, "A nonlinear observer approach of SOC estimation based on hysteresis model for lithium-ion battery," *IEEE/CAA Journal of Automatica Sinica*, vol. 4, no. 2, pp. 195−204, Apr. 2017.

Y. Ma and H. Chen are with the State Key Laboratory of Automotive Simulation and Control, Jilin University, Changchun 130012, China, and also with the Department of Control Science and Engineering, Jilin University (Campus Nanling), Changchun 130025, China (e-mail: yma@jlu.edu.cn; chenh98cn@126.com).

B. S. Li and G. Y. Li are with Jilin University, Changchun 130012, China (e-mail: lbsmichelle@163.com; 18204312059@163.com).

J. X. Zhang is with Beijing Institute for Control and Electronic Technology, Beijing 100038, China (e-mail: jixiangyu318@126.com).

Color versions of one or more of the figures in this paper are available online at http://ieeexplore.ieee.org.

Digital Object Identifier 10.1109/JAS.2017.7510502

of these battery systems require an appropriate battery model [6]. In [17], we can see that the battery parameters, such as internal resistance, can be different in different charging and discharging rates or other conditions. So it is necessary for us to build a more accurate battery model such as parameter-varying model with hysteresis effect.

The hysteresis constitutes a very significant internal variable for some battery technologies. Its value depends on the battery process, which can be divided into three possibilities: charging, discharging and charging/discharging transient. There is not yet a clear physical explanation for the hysteresis phenomenon, although the domain theory relates the hysteresis to separated regions inside the electrode that lead to different electrode equilibrium potentials during the charging and discharging [18], [19]. The hysteresis phenomenon also modifies the model parameters of the battery and therefore its dynamic response [20]. So we consider the influence of hysteresis on the OCV of the battery in charging/ discharging transient.

Therefore, the future study on SOC estimation will focus not only on highly accurate and strongly robust estimation methods, but also on modeling the cell accurately by means of studying the battery characteristics.

The remaining part of the paper is organized as follows. In Section II an equivalent circuit model with hysteresis (ECMH) is presented to characterize the dynamics of lithium-ion cell, and the detail procedures to identify the battery ECM parameters are also explained. In Section III, the nonlinear observer based on the ISS theory is proposed to estimate SOC of lithium-ion cell. The numerical algorithm for SOC estimation based on the nonlinear observer is verified by the co-simulation in Matlab/Simulink and AMESim respectively in Section IV. Finally, conclusions are given in Section V.

## II. Hysteresis Modeling and Parameter Identification

In this section, the simplified equivalent circuit model with the hysteresis characteristic of lithium-ion cell will be modeled. Time-varying elements in each RC network and the internal resistance are considered. The hysteresis element in the equivalent circuit model shows the nonlinear characteristics of the components inside the SOC estimating system [21].

### A. Hysteresis Modeling of Lithium-ion Cell

The motion of the lithium-ion in the cell is shown in Fig. 1. The equivalent circuit model with hysteresis characteristic of lithium-ion cell is shown in Fig. 2.

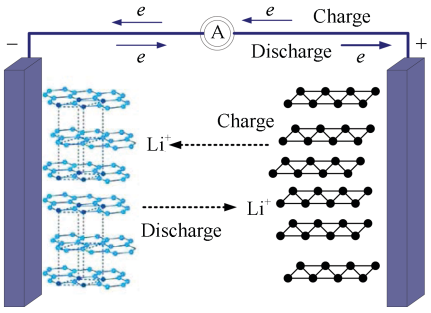


Fig. 1. Lithium-ion battery schematics.

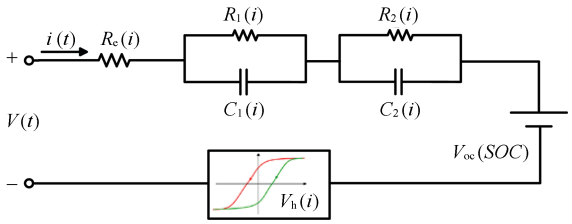


Fig. 2. Equivalent circuit model with hysteresis.

This model consists of an ohmic internal resistance $R_{\rm e}(i)$, two RC networks ($R_1(i)$, $C_1(i)$ represent the electrochemical polarization effect, $R_2(i)$, $C_2(i)$ represent the concentration polarization effect), and a hysteresis link $V_{\rm h}(i)$.

According to Kirchhoff's law, the terminal voltage can be given by

$$V = V_{\rm oc}(SOC) + V_1 + V_2 + V_h + R_{\rm e}(i)\cdot i \tag{1}$$

and the electrochemical polarization voltage $V_1$ and the concentration polarization voltage $V_2$ can be expressed as

$$\dot{V}_1 = -\frac{1}{R_1C_1}V_1 + \frac{1}{C_1}i \tag{2}$$

$$\dot{V}_2 = -\frac{1}{R_2C_2}V_2 + \frac{1}{C_2}i \tag{3}$$

where $V_{\rm oc}$ is the OCV; $V_1$ is the voltage of network of $R_1C_1$, $V_2$ is the voltage of network of $R_2C_2$; $V_{\rm h}$ is the voltage of hysteresis part; $R_{\rm e}$ is the ohmic internal resistance and $i$ represents the instantaneous current ($i>0$ means charge process of the battery, while $i<0$ means discharge process of the battery). $\tau_1 = R_1C_1$ and $\tau_2 = R_2C_2$ are the time constants.

The OCV, as a function of SOC, is simplified as $V_{\rm oc}(SOC)$, which can be expressed [22] as

$$V_{\rm oc}(SOC) = \lambda\cdot V_{\rm oc}^{\rm C}(SOC) + (1-\lambda)\cdot V_{\rm oc}^{\rm D}(SOC) \tag{4}$$

where $\lambda\in(0,1)$, is proportionality coefficient. $V_{\rm oc}^{\rm C}(SOC)$ and $V_{\rm oc}^{\rm D}(SOC)$ is the OCV of the charge and discharge of a battery at this SOC, respectively. Once the parameter $\lambda$ is determined, we could get the OCV value corresponding to this SOC.

The hysteresis voltage $V_{\rm h}$ is a first order dynamic process [23] related to current absolute value, which can be expressed as

$$\dot{V}_{\rm h} = (1-e^{-|\kappa\cdot i|})V_{\rm h} \pm (1-e^{-|\kappa\cdot i|})H \tag{5}$$

where $\kappa$ is the attenuation coefficient, $H$ can be expressed as (9), which is the upper bound of hysteresis voltage determined by charging/discharging OCV, and $\pm$ represent charging and discharging, respectively.

$$H = \frac{1}{2}[V_{\rm oc}^{\rm C}(SOC) - V_{\rm oc}^{\rm D}(SOC)]. \tag{6}$$

Choose state variables as $x = \begin{bmatrix} SOC & V_{\rm h} & V_1 & V_2\end{bmatrix}^T$. Let input as $u = \begin{bmatrix} i & \pm H\end{bmatrix}^T$, current $i$ and hysteresis voltage's upper bound $H$. Let the output as $y = V$. Then state space model is shown as follows

$$\dot{x} = A(i)\cdot x + B(i)\cdot u \tag{7}$$

$$y = g(x) + D(i)\cdot u \tag{8}$$

where $A(i) = \begin{bmatrix} 0 & 0 & 0 & 0 \\ 0 & 1-e^{-|\kappa \cdot i|} & 0 & 0 \\ 0 & 0 & -\frac{1}{R_1(i)C_1(i)} & 0 \\ 0 & 0 & 0 & -\frac{1}{R_2(i)C_2(i)} \end{bmatrix}$

$$B(i) = \begin{bmatrix} \frac{1}{Q_N} & 0 \\ 0 & 1-e^{-|\kappa \cdot i|} \\ \frac{1}{C_1(i)} & 0 \\ \frac{1}{C_2(i)} & 0 \end{bmatrix}, \quad D(i) = \begin{bmatrix} R_e(i) & 0 \end{bmatrix}$$

$g(x) = V_{oc}(SOC) + V_h + V_1 + V_2$. And $R_1(i)$, $R_2(i)$, $C_1(i)$, $C_2(i)$, $R_e(i)$ represents the dependency of these parameters on current.

### *B. Model Parameterization Identification*

The cell characterization and validation tests are carried out on single cell. The 2.5 Ah cells are used for experiment in this paper. The OCV boundary curve test and hysteresis test are done on a Neware battery test device BTS-5V6A that comprises a voltage measurement accuracy of ±5 mV and a current measurement accuracy of ±6 mA (of the full scale value). During testing the cells, ambient temperature is constantly held at 25 °C.

The model parameterization test schedule includes cell capacity test and OCV test. The first charging circulation of the cells makes the cells' chemical characteristics fully activated.

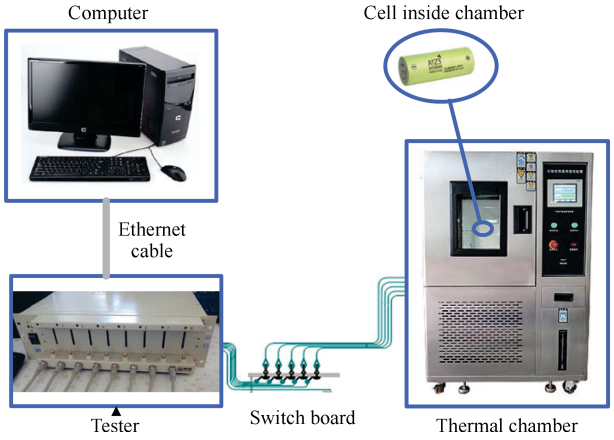


Fig. 3. Configuration of the battery test bench.

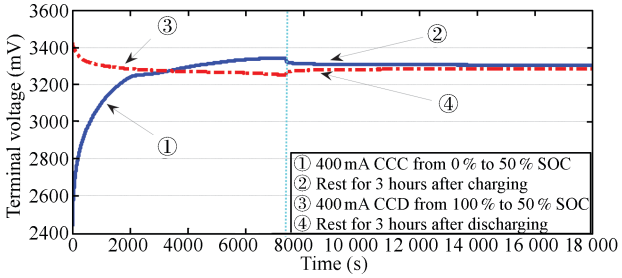


Fig. 4. Battery charge and discharge rest curve.

During the first OCV test (boundary curve test), the cells are gradually discharged in 10 % ΔSOC steps beginning at SOC = 100 %, with constant current 0.25 C, which means 400 mA, until reaching the discharge cutoff voltage (2 V). Then the cells are recharged again (10 % interval, 0.25 C). And then, equivalent resistance, polarization resistance and polarization capacitance are identified in this section.

The charging and discharging idle curve of the battery test is shown in Fig. 4, in which there are two curves. One is the charging segment ① and charging idle segment ②. The other is the discharging segment ③ and idle segment ④.

Segment ① shows the charging process with SOC 0 % to 50 %; segment ② shows that the battery has been rested for 3 hours;

Segment ③ shows the discharging process with SOC 100 % to 50 %; segment ④ also shows that the battery has been rested for 3 hours;

Segment ④ is calibrated as shown in Fig. 5, where the initial point is set at zero for simply curve fitting. Here exponential function is taken to fit parameters of battery terminal voltages.

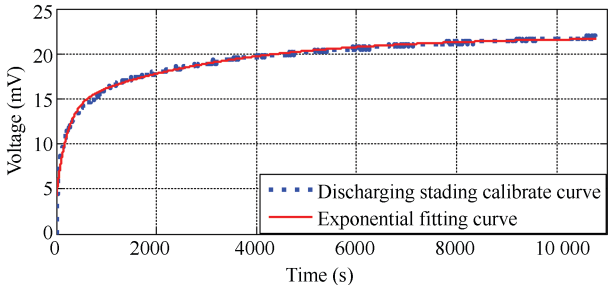


Fig. 5. Fitting curve of Segment ④.

According to the circuit relations in Fig. 1 and (1)−(3), we can get the battery terminal voltage output equation as follows

$$V = V_{oc} + R_e i + R_1 i(1 - e^{-t/\tau_1}) + R_2 i(1 - e^{-t/\tau_2}). \quad (9)$$

Then we choose the exponential fitting function expression as

$$V = k_0 + k_1 e^{-\lambda_1 t} + k_2 e^{-\lambda_2 t} \quad (10)$$

where $k_0$, $k_1$, $k_2$ are constants; $\lambda_1$, $\lambda_2$ are the time constants. Writing an exponential fitting function in MATLAB with the rest voltage curves as shown in Fig. 4, we can determine the parameters $k_0$, $k_1$, $k_2$, $\lambda_1$ and $\lambda_2$, and obtain the fitting curve like Fig. 5. And then the model parameters $R_e$, $R_1$, $R_2$, $C_1$ and $C_2$ can be determined accordingly.

In order to study the effect of charge and discharge current of battery on the model parameters, we had taken 16 sets of charging/discharging experiments, and 100 times per set. Discharging currents are −1600 mA to −200 mA, and charging currents are 200 mA to 1600 mA, with 200 mA interval current. Fitting the charging/discharging rest curve, the values of equivalent internal resistance, polarization resistances and polarization capacitances are shown in Table I.

The second OCV test is for investigating the hysteresis effect.

Gradual partial cycles are applied to achieve the intermediate OCV curves between the OCV boundary curves as shown in Fig. 6. At first the cells (SOC = 0 %) are charged to SOC = 50 %. After 3 hours rest, the cells are discharged by ΔSOC = 10 % for four times (SOC = 10 % with 0.25 C and rest 3hours a time after discharging). Then the cells are charged again in four steps (10 % SOC a time, 0.25 C). The same cycles

are repeated for initial SOC = 50 % and 10 %, respectively. The nominal capacity is extracted from the cells being constant current constant voltage (CCCV) charged previously.

From Fig. 6 we can see that the OCV value changes through the hysteresis belt from the charging curve into discharging curve. We can get the maximum value of $H$ in different SOC values [24], i.e., $H = 13$ mV by computing (6), and determine $\kappa = 4 \times 10^{-6}$ by curve fitting the terminal voltage function in (1) and (5).

TABLE I
THE RELATION BETWEEN MODEL PARAMETERS AND CHARGE- & DISCHARGE-CURRENT

| No | $i$(A) | $R_e(\Omega)$ | $R_1(\Omega)$ | $R_2(\Omega)$ | $C_1(F)$ | $C_2(F)$ |
|---|---|---|---|---|---|---|
| 1 | –1.6 | 0.0397 | 0.0220 | 0.0052 | 3245.3 | $2.8182\times10^5$ |
| 2 | –1.4 | 0.0399 | 0.0227 | 0.0060 | 3330.4 | $2.4293\times10^5$ |
| 3 | –1.2 | 0.0405 | 0.0237 | 0.0068 | 3519.4 | $2.2674\times10^5$ |
| 4 | –1.0 | 0.0434 | 0.0242 | 0.0120 | 5684.6 | $1.9716\times10^5$ |
| 5 | –0.8 | 0.0421 | 0.0252 | 0.0091 | 4120.9 | $2.2000\times10^5$ |
| 6 | –0.6 | 0.0428 | 0.0267 | 0.0111 | 4381.1 | $1.7728\times10^5$ |
| 7 | –0.4 | 0.0424 | 0.0229 | 0.0236 | 10219 | $1.2599\times10^5$ |
| 8 | –0.2 | 0.0457 | 0.0261 | 0.0415 | 9410.3 | $9.7443\times10^4$ |
| 9 | 0.2 | 0.0587 | 0.0356 | 0.0346 | 9300.8 | $1.0908\times10^5$ |
| 10 | 0.4 | 0.0473 | 0.0249 | 0.0195 | 8475.9 | $1.6055\times10^5$ |
| 11 | 0.6 | 0.0415 | 0.0240 | 0.0119 | 4021.7 | $1.9176\times10^5$ |
| 12 | 0.8 | 0.0407 | 0.0225 | 0.0095 | 3826.5 | $2.2920\times10^5$ |
| 13 | 1.0 | 0.0385 | 0.0201 | 0.0061 | 3303.7 | $2.3189\times10^5$ |
| 14 | 1.2 | 0.0398 | 0.0206 | 0.0066 | 3570.0 | $3.4728\times10^5$ |
| 15 | 1.4 | 0.0392 | 0.0200 | 0.0059 | 3375.6 | $3.8511\times10^5$ |
| 16 | 1.6 | 0.0387 | 0.0194 | 0.0054 | 3101.6 | $3.7891\times10^5$ |

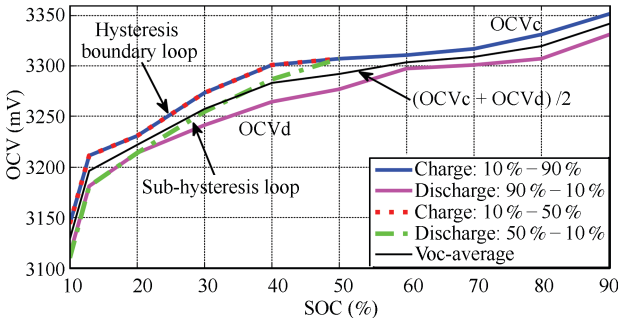


Fig. 6. Charging/discharging OCV curves.

### C. Model Verification

To verify the accuracy of this parameter-varying second order RC ECHM, build the battery simulation model in MATLAB/Simulink. Charge the battery from SOC 0 % to 50 % by constant current of 400 mA, and then discharge it to SOC 10 % by the same current. We get battery terminal voltage shown in Fig. 7 and the errors between model and measured voltage are shown in Fig. 8. Those figures tell us that the error mainly remains under 10mV when SOC = 10 % – 50 %. The part of SOC below 10 % is ignored in parameter calibration because of unstable performance, complex process, and rare use of battery in this condition, while we ensure the high accuracy in other conditions.

To verify the accuracy and reliability of the model in complex process, design a current-varying procedure as shown in Fig. 9, which contains current value switching and charging-discharging switching. We contrast the voltage output of this model and a first order RC model with the measured values, and get the results as in Figs. 10 and 11.

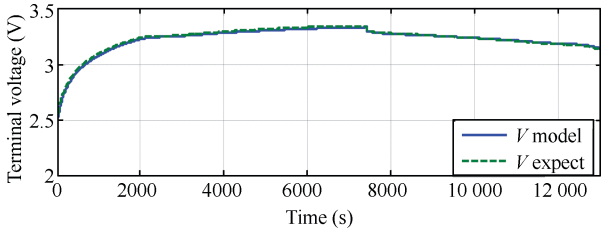


Fig. 7. The parameter-varying second order RC equivalent circuit model with hysteresis simulation verification results.

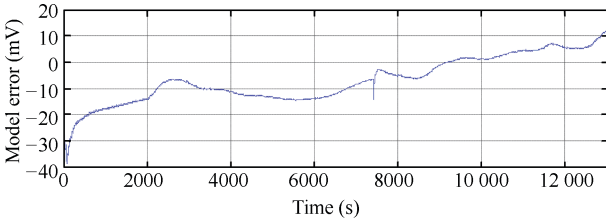


Fig. 8. Battery model error.

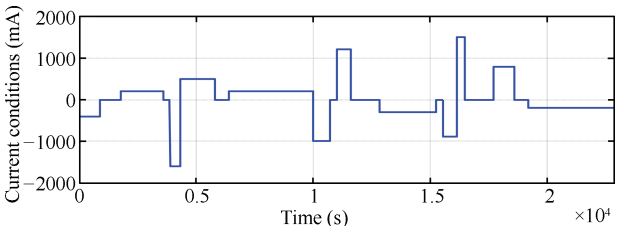


Fig. 9. Custom current conditions.

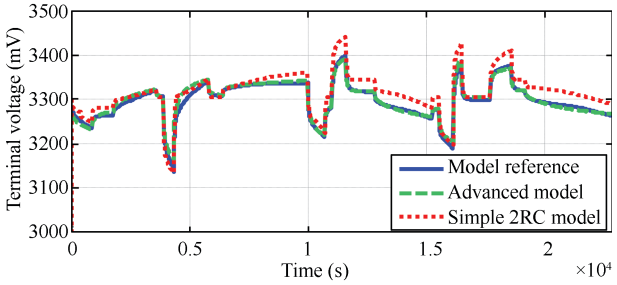


Fig. 10. Battery model verification results.

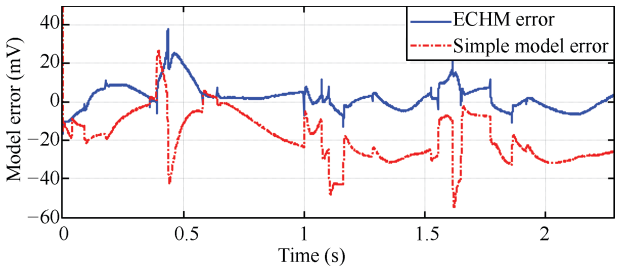


Fig. 11. Battery model error under custom current conditions.

The voltage output values of the two models and the

measured voltage are shown in Fig. 12. And the output errors of the two models are shown in Fig. 13. And those figures tell us obviously that the errors of parameter-varying model with hysteresis characteristics mainly remain under 10 mV, which is a great improvement in accuracy than the first order one. In addition, the tracking performance progresses a lot as well especially when charging-discharging switching.

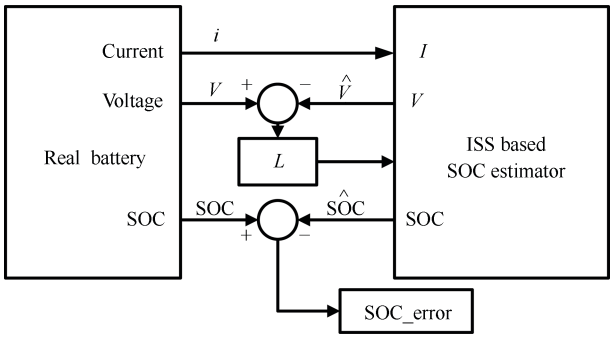


Fig. 12. ISS based observer simulation model block diagram.

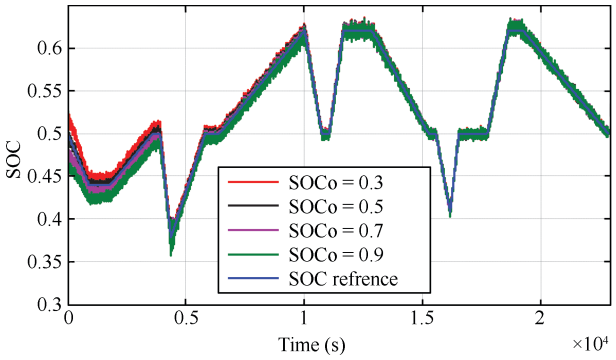


Fig. 13. The SOC estimation effect validation of the nonlinear observer.

The simulation results show that the accuracy and other model characters could be improved by adding into the model the consideration of the difference between charging and discharging process and the influence of the current on the coefficients. Besides, the errors of the two models both increase when charging-discharging switching, but the addition of hysteresis influence would make the model better simulate the real response when switching and keep the error at about 10 mV.

## III. ISS Based Nonlinear Observer

In this section, the parameter uncertainties and unmodeled dynamics are considered as disturbance inputs, and it can be proved that the SOC estimating closed-loop error system has robust stability based on the ISS theory.

### A. ISS Stability Analysis

To analyze the ISS stability of the SOC estimator of battery, we rewrite the dynamic system (7) and (8) as follows

$$\dot{x} = A(i) \cdot x + B(i) \cdot u + w \tag{11}$$

$$y = g(x) + D(i) \cdot u + v \tag{12}$$

where $w$ and $v$ summarize the model uncertainties and the output measurement noise, respectively. The model parameters come from a series of modeling experiments in Section II, and the observer system is observable.

The nonlinear observer is designed in the form of

$$\dot{\hat{x}} = A(i) \cdot \hat{x} + B(i) \cdot u + L(y - \hat{y}) \tag{13}$$

$$\hat{y} = g(\hat{x}) + D(i) \cdot u \tag{14}$$

where $L \in \mathbb{R}^{4\times 1}$ is the observer gain to be determined later.

The observer error is defined as follows

$$e = x - \hat{x} \tag{15}$$

then the error dynamics are described by

$$\begin{aligned} \dot{e} &= A(i)x + B(i)u + w - A(i)\hat{x} - B(i)u - L(y - \hat{y}) \\ &= A(i)e + w - L[g(x) - g(\hat{x})] - Lv \end{aligned} \tag{16}$$

where $g(x)$ can be rewritten as the linear equation

$$g(x) - g(\hat{x}) = C(x) \cdot x - C(\hat{x}) \cdot \hat{x} + o(x). \tag{17}$$

Substituting (17) into (16) leads to

$$\begin{aligned} \dot{e} &= [A(i) - LC(\hat{x})]e + w - L[\Delta C x + o(x) + v] \\ &= [A(i) - LC(\hat{x})]e + w - Lw_1 \end{aligned} \tag{18}$$

where $\Delta C = C(x) - C(\hat{x})$, $\Delta C x + o(x) + v = w_1$.

Let the candidate Lyapunov function be in the form

$$V = \frac{1}{2} e^T P e \tag{19}$$

with positive definite symmetric matrix $P$.

The time derivative of (19) is

$$\begin{aligned} \dot{V} &= \frac{1}{2}[\dot{e}^T P e + e^T P \dot{e}] \\ &= \frac{1}{2}[e^T (A(i)^T P - C(x)^T L^T P + PA(i) - PLC(x))e] \\ &\quad + \frac{1}{2}(w^T P e - w_1^T L^T P e + e^T P w - e^T P L w_1). \end{aligned} \tag{20}$$

Let $PL = Q$, using $P^T = P$, and $P$ is a positive definite symmetric matrix, so there must be an orthogonal matrix $U$ and a diagonal matrix $\Lambda$ making $P = U\Lambda U^{-1}$, where $\Lambda = \mathrm{diag}(\sqrt{a_{ii}})^2 = {\Lambda_1}^2$. Then $P = (U\Lambda_1 U^{-1})^2 = P_1^2$. Define $P_1 w = v_1$, $P_1 L w_1 = v_2$ and $v_0 = v_1 - v_2$ , then (20) becomes

$$\begin{aligned} \dot{V} &= \frac{1}{2}[e^T (A(i)^T P - C(x)^T Q^T + PA(i) - QC(x))e] \\ &\quad + (P_1 e^T) v_0. \end{aligned} \tag{21}$$

Apply Young's Inequality [15] to achieve

$$(P_1 e^T) v_0 \le \kappa_1 e^T P e + \frac{1}{4\kappa_1} v_0^T v_0 \tag{22}$$

where $\kappa_1 > 0$.

Then (21) becomes

$$\begin{aligned} \dot{V} = \frac{1}{2}\Big[ & e^T (A(i)^T P - C(x)^T Q^T + PA(i) \\ & - QC(x) + 2\kappa_1 P)e\Big] + \frac{1}{4\kappa_1} v_0^T v_0. \end{aligned} \tag{23}$$

Choose $P$, $Q$ to satisfy the following inequality

$$A(i)^T P - C(x)^T Q^T + PA(i) - QC(x) + 2\kappa_1 P \le -\kappa_2 P \tag{24}$$

with $\kappa_2 > 0$.

Then (23) becomes

$$\dot{V} \leq -\frac{1}{2}\kappa_2 e^T P e + \frac{1}{4\kappa_1} v_0^T v_0. \tag{25}$$

Substitute (19) into (25), we have

$$\dot{V} \leq -\kappa_2 V + \frac{1}{4\kappa_1} v_0^T v_0. \tag{26}$$

Using the fact that [13]

$$\frac{1}{2}\lambda_{\min}(P)\|e\|^2 \leq \frac{1}{2} e^T P e \leq \frac{1}{2}\lambda_{\max}(P)\|e\|^2 \tag{27}$$

where $\lambda_{\min/\max}(P)$ denotes the minimum/maximum eigenvalue of the matrix $P$.

From (25) and (26), we have

$$\dot{V} \leq -\frac{1}{2}\kappa_2 \|e\|^2 \sup \lambda_{\max}(P) + \frac{1}{4\kappa_1}\|v_0\|^2. \tag{28}$$

Upon multiplication of (26) by $e^{\kappa_2 t}$, we get

$$\frac{d}{dt}(V e^{\kappa_2 t}) \leq \frac{1}{4\kappa_1} v_0^T v_0 e^{\kappa_2 t}. \tag{29}$$

Integrating (29) over the interval $t \in [0, t]$, then

$$V(t) = V(0)e^{-\kappa_2 t} + \frac{1}{4\kappa_1}\int_0^t e^{-\kappa_2(t-\tau)} v_0^T v_0 d\tau \tag{30}$$

Hence, the properties of the error dynamics of the designed observer (13) and (14) are described as follows.

*Theorem 1:* Suppose the following:

1) $\kappa_1 > 0$, $\kappa_2 > 0$;

2) The observer gain $P$, $Q$ is chosen to satisfy (24).

Then, the error dynamic property of the observer (13) and (14) are as follow:

1) Input-to-state stable, if $w$ and $w_1$ are bounded in amplitude, i.e., $w, w_1 \in \mathcal{L}_\infty$;

2) Exponentially stable with $\kappa_2$ for $w = w_1 = 0$.

*Proof:* It follows from (25) to (30), which shows that the error dynamics admit the input-to-state stability property if the model error $w$ and $w_1$ are supposed to be bounded in amplitude, as property 1) required.

Taking $w = w_1 = 0$, which means $v_1 = v_2 = 0$, and $v_0 = 0$, we obtain from (30) that $|e(t)| \leq |e(0)|e^{-\kappa_2 t}$, $\forall t \geq 0$ which proves property 2). ■

*Remark 1:* Now we give some discussions on the parameters $\kappa_1$ and $\kappa_2$. From property 2), $\kappa_2$ is chosen according to the required decay rate of the error. If $w$ and $w_1$ are bounded in amplitude, i.e., $w, w_1 \in \mathcal{L}_\infty$, then (30) becomes

$$\|e(\infty)\|^2 \leq (\frac{\|v_0\|_\infty^2}{4\kappa_1}) \lim_{t\to\infty} \int_0^t e^{-\kappa_2(t-\tau)} d\tau \tag{31}$$

i.e.,

$$\|e(\infty)\|^2 \leq \frac{\|v_0\|_\infty^2}{4\kappa_1\kappa_2}. \tag{32}$$

Hence, one may choose larger $\kappa_1$ to reduce the offset. From (24), however, one also notices that the larger $\kappa_1$ is, the higher observer gain is [15].

*Remark 2:* Equation (32) gives just an upper bound of the estimation error offset, if the bound of the model error is given. The real offset could be much smaller, due to the multiple use of inequalities in the above derivation.

### B. Implementation Issues and SOC Observer Design

According to Theorem 1 and Remark 1, a systematic procedure is given to design the ECHM based observer in the form of (13), Equation (14) as follows, and the observer gain satisfies (24).

*Step 1:* Choose the parameter $\kappa_2$, according to the required error decay rate of the estimation error;

*Step 2:* Choose the parameter $\kappa_1$, where it is suggested to start from some smaller values (according to Remark 1);

*Step 3:* Determine the observer gain $L$ and make it satisfy (24);

*Step 4:* Use (32) to compute the estimated upper bound of the offset for a given model error bound, and check if the offset bound is acceptable;

*Step 5:* If the offset bound is acceptable, end the design procedure. If not acceptable, go to Step 2.

It is well known that getting model error bounds is in general very difficult, if not impossible. As mentioned in Remark 2, for a given model error bound, (32) gives just an upper bound of the estimation error offset, but the calculation of static error after continuous inequality arithmetic might be much larger than the real offset. Hence, the stopping of iterations from Steps $1-5$ is somehow a "rule of thumb", and we can obtain the most appropriate gain after repeated calculation [16].

We now give a solution of (24) for choosing $L$ to be time-invariant (constant value), where the requirement for low observer gains can be considered through linear matrix inequality (LMI) optimization method. If $A(i)$ and $C(x)$ in (24) vary in a polytope (convex polyhedron) with $r$ vertices, i.e.,

$$(A(i) \;\; C(x)) \in Co\{(A_1 \;\; C_1), (A_2 \;\; C_2), \ldots, (A_r \;\; C_r)\} \tag{33}$$

where $Co\{\}$ denotes the convex hull of the polytope. Then, there are

$$\beta_1, \beta_2, \ldots, \beta_r \geq 0 \tag{34}$$

that satisfy

$$\sum_{n=1}^{r} \beta_n = 1 \tag{35}$$

and make

$$(A(i) \;\; C(x)) = \sum_{n=1}^{r} \beta_n (A_n \;\; C_n). \tag{36}$$

Hence, conclusions are given as follows.

*Theorem 2:* Suppose that $A(i)$ and $C(x)$ vary in a polytope as (33). Then for any time-invariant $P$, $Q$ satisfying the following linear matrix inequalities (LMIs):

$$\begin{gathered} A_n^T P - C_n^T Q^T + P A_n - Q C_n + 2\kappa_1 P + \kappa_2 P \leq 0 \\ n = 1, 2, \ldots, r \end{gathered} \tag{37}$$

meet the observer gain condition (24).

*Proof:* The substitution of (36) into (24) leads to

$$\sum_{n=1}^{r} \beta_n (A_n^T P - C_n^T Q^T + P A_n - Q C_n + 2\kappa_1 P + \kappa_2 P) \leq 0. \tag{38}$$

Due to (35), the satisfaction of (37) guarantees (24) and hence (38).

According to (35), if (37) is satisfied, (24) and (38) must be valid. ■

In (37), $A_n$ and $C_n$ are known and bounded, $\kappa_1$ and $\kappa_2$ are selected to be bounded, hence, some constant $L$ is always found to render it satisfying, i.e., $P$, $Q$ is always satisfying (37). Moreover, we prefer to have low observer gains, for being robust against noises and reducing the upper bound of the error offset, which is estimated by (32). Hence, $L$ is obtained through $L = P^{-1}Q$.

By solving LMIs optimization problem (37), the solution gives then a constant observer gain with the lowest possible values satisfying the condition (24).

Under different circuit working conditions, $A_n$ and $C_n$ are computed respectively, then the optimal $P$ and $Q$ are solved through the LMI toolbox of Matlab, and the optimal observer gain $L$ is calculated.

$$P = \begin{bmatrix} 4.1921 & 0.0636 & -0.0048 & 0.0402 \\ 0.0636 & 0.0011 & -1.0366e^{-5} & 6.1983e^{-5} \\ -0.0048 & -1.0366e^{-5} & 1.6871 & -4.8214e^{-5} \\ 0.0402 & 6.1983e^{-5} & -4.8214e^{-5} & 3.8635e^{-5} \end{bmatrix} \tag{39}$$

$$Q = \begin{bmatrix} 0.0048 & 4.3605e^{-5} & 3.7697e^{-5} & 4.3146e^{-5} \end{bmatrix}^T \tag{40}$$

then the observer gain is

$$L = P^{-1}Q = \begin{bmatrix} 0.1553 & 0.8038 & -1.9750 & 17.3426 \end{bmatrix}^T.$$

### C. Simulation Results

The proposed ISS based SOC observer is verified by AMESim/Simulink co-simulation. First the observer is programmed in MATLAB/Simulink as in Fig. 12. Then a simulation model of EV is developed in AMESim environment. The model's parameters are configured based on driving cycles and the lithium-ion batteries used in this paper, so that the battery module within will capture the transient dynamics.

Before simulation, set up the initial value of battery model SOC as 50 %, and the initial values of nonlinear observer SOC as 30 %, 50 %, 70 %, 90 %, to verify the estimation precision of the observer under the inaccurate SOC initial values. Plots in Fig. 13 gives the simulation results of the SOC with the current condition of Fig. 9, i.e., the condition for the observer design. In Fig. 13 the red, black, purple and green curves are the observer output SOC estimations, the blue curve is SOC reference value. Due to the simulation is run for a long time, the experimental data volume is larger, so we zoom in the former 2000 s of the simulation results, as shown in Fig. 14. We can see from Fig. 14, at the start of the simulation, SOC estimation has different initial errors with reference value, but at the beginning of the simulation within 1000 s, SOC estimate is gradually moving closer to the "true SOC value". In practice, the requirement of convergence rate of SOC estimation is not very high, so we think estimation error convergence within 1000 s meets the actual requirements here.

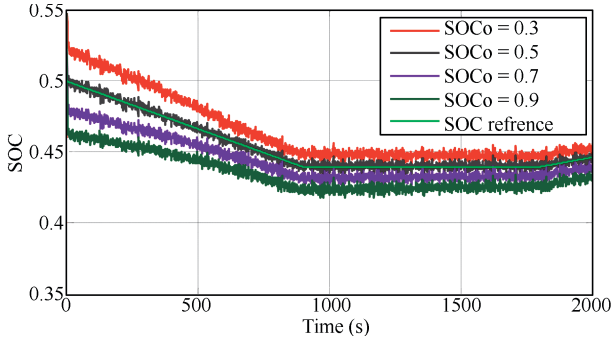


Fig. 14. Detailed SOC estimation simulation before the 2000s.

In Fig. 15, SOC estimation error and detailed simulation before the 2000 s are shown, and we can see that, the observer estimation error is within 2 % and does not diverge throughout the operation. Those simulation experiments prove that the observer has a good robustness. At this point, we prove that the calculated observer gain in Section III-C can make estimation error meet the ISS from theoretical analysis and simulation experiment respectively.

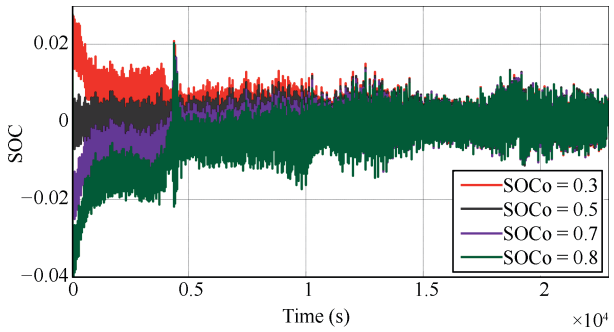


Fig. 15. SOC estimation error.

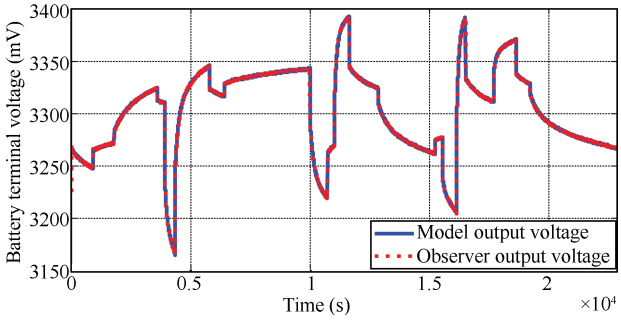


Fig. 16. Nonlinear observer battery terminal voltage estimation effect verification.

Fig. 16 shows the comparison curve of the output voltage for the nonlinear observer and the terminal voltage of battery model. In Fig. 16 the red curve is the terminal voltage estimation value of the battery model, the blue curve is the terminal voltage of battery model with white noise, to simulate the actual sensor measurement noise. The resolution of the experimental equipment is 5 mV, the white Gaussian noise added into this simulation experimentation is with the average of 0, and the variance of 0.25. Hence, the estimation performance in Fig. 13 to Fig. 16 is much better. In the custom current conditions, the observer can accurately track the voltage of

the battery, which shows that the observer can guarantee the precision of SOC estimation, at the same time, and can accurately estimate the other three state variables.

## IV. The Observer Verification Based on AMESim

The proposed ISS based SOC observer is verified by AMESim/Simulink co-simulation. First the observer is programmed in Matlab/Simulink as in Fig. 10. Then a simulation model of EV is developed in AMESim environment. The model's parameters are configured based on driving cycles and the lithium-ion batteries used in this paper, so that the built-in battery module will capture the transient dynamics.

Electric vehicle model and the battery module in AMESim are shown in Fig. 17.

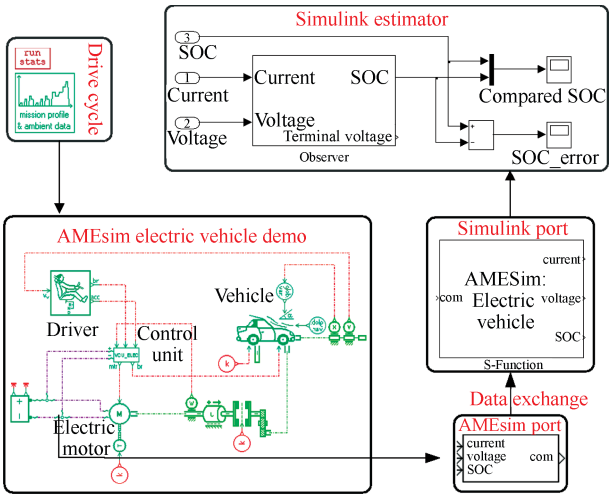


Fig. 17. AMESim/Simulink co-simulation sketch.

We set up the co-simulation environment, and the AMESim/Simulink co-simulation flow chart is shown in Fig. 17. All the model ports allow parameter configuration. So before simulation, we need to load the relation between the battery's internal parameters (resistance $R$ and open circuit voltage $V_{oc}$) and the depth of discharge (DOD = 1−SOC) to the software installation location specified directory. The relation between OCV and DOD is given by battery OCV boundary test in Section II. The relation between the battery's internal resistance $R$ and DOD is obtained from the impulse charging/discharging test. The test is conducted between 0 % and 100 % at every 5 % SOC interval to obtain the battery internal resistance.

In practice, the cell obviously cannot provide the driven motor with sufficient voltage and current, so we need to make battery packs which can be series or parallel connected in several sets [9]. In the process of vehicle modeling, we changed the battery module parameters into the A123-26650 battery which is studied and completely calibrated. We set that the battery module contains 40 series battery unit and every battery unit contains 100 parallel cells. At this point, the electric vehicle battery module is set completely.

In this paper we choose New European driving cycle (NEDC) which lasts for 1180 s. This driving cycle is a typical procedure for light-duty vehicle (less than 3500 kg) under European emission standards. It consists of 4 urban cycles and an expressway cycle (urban speed under 50 km/h, expressway speed under 120 km/h, frequent start-stop state), and the whole process lasts 20 minutes. The details of the procedure are shown in Fig. 18.

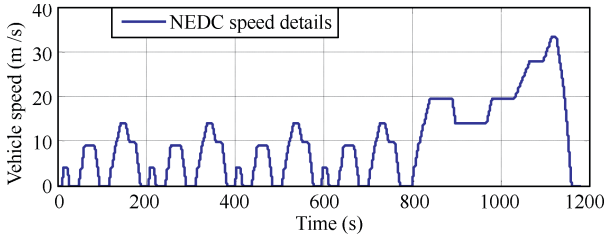


Fig. 18. NEDC speed working condition details.

We need to verify if the precision of the battery model is satisfied in AMESim before SOC estimation. If the model accuracy meets the requirements, co-simulate to estimate battery SOC and to verify the accuracy of the estimation algorithm under the actual working condition. If it does not meet the precision requirements, then we need to adjust model parameters.

Under AMESim environment, set up the cycle condition as NEDC, and the initial value of battery SOC at 80 %. The working condition of cell is shown in Fig. 19, which is corresponding to the car speed details. When speed is low, discharge current is small; When the car is idle, the current is zero; When the car speed is up, discharge current instantaneously increases; When the car is braking, the motor mode changes into electric generator mode and charges the battery.

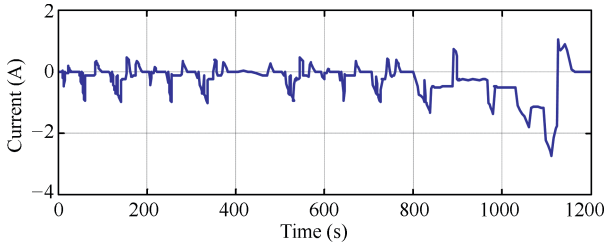


Fig. 19. Working current of the cell under NEDC.

The current value of the working condition and charge/discharge switches frequently comparing the forestall custom condition, and it is in favor of validating battery model's accuracy in complex current conditions. The terminal voltage of cell in the battery pack through the simulation experiment is shown as the blue curve in Fig. 20. After fine-tuning the parameters of the model established in Section II, we get the output voltage of the battery model shown as the red dotted line in Fig. 20. The battery model error is shown in Fig. 21.

Within the simulation time of 0 s−800 s, i.e., under the city working condition, the battery working current is relatively small, and the model error is within 15 mV; Later in the simulation, the car went into the high speed cycle, and the battery charge/discharge current increases. The error of the parameter identification resulted in the model error increased in this period. When the discharge current increases instantaneously, the model error value is up to 26 mV. Throughout the whole working condition cycle, by removing the influence of the individual "spine" points, the model error can keep

within 15 mV, which means the model accuracy meets the requirements.

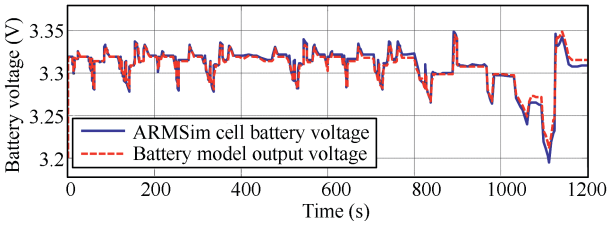


Fig. 20. Verification of the Li-ion battery under AMESim environment.

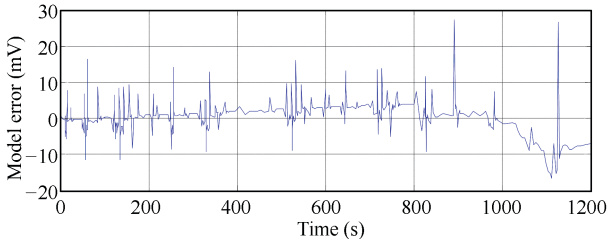


Fig. 21. Modeling error of the Li-ion battery under AMESim environment.

After the model verification, we would test the SOC estimation accuracy of the proposed nonlinear observer under complex current procedure. Link AMESim and Simulink according to Fig. 17, set the charging-discharging current as is shown in Fig. 18, and set the SOC initial value $80\,\%$ to operate co-simulating. Use the SOC output from AMESim battery value as the "true value". The SOC accuracy would be tested with model errors.

The battery working current and SOC value constantly changes along with the vehicle's start-stop, accelerating and braking. In urban cycle, the maximum discharging current is 40 A, while in expressway cycle it reaches 110 A. The battery's terminal voltage changes with current, but the range is limited within 10 V because of the flat voltage plateau of LiFePO4 batteries. With the observer's SOC initial value set at $82\,\%$ before simulation, we get the estimation result shown in Fig. 22 and the estimation error curve in Fig. 23. After simulation, the battery SOC value decreases from $80\,\%$ to $76.4\,\%$. In addition, we put a plenty of battery packs in parallel so as to have relatively small current in each pack, which would reduce the battery heat generation [25], [26] and cut down the polarization current to improve the service time of one charging.

We set the observer with different SOC initial values in the AMESim battery model, because of the difficulty in determination of SOC initial value in application, and to verify the proposed observer's high accuracy, good robustness and the ability to overcome the incorrect initial value problem. In the beginning of simulation, the observer constantly corrects the error between estimation value and "true value". And then with the influence of model error, it keeps the estimation value waving near "true value" by correction. Finally, considering all the results of the whole cycle procedure, we get the SOC estimation error within $1.1\,\%$, which represents high accuracy.

The simulation results show that the proposed ISS observer can not only guarantee the convergence of estimation error,

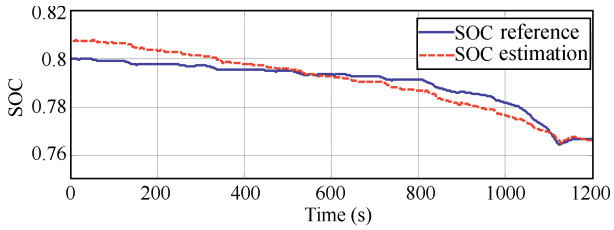


Fig. 22. SOC estimation of Li-ion battery pack under NEDC.

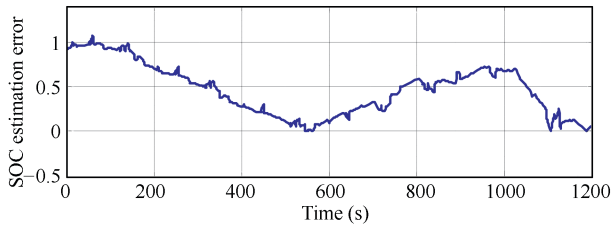


Fig. 23. SOC estimation error of Li-ion battery pack under NEDC.

but also effectively overcome the error of incorrect SOC initial value. Furthermore, the nonlinearity causing divergence can be effectively overcome in real vehicle running for the model nonlinearity is sufficiently taken into consideration during ISS observer design. Therefore, we believe that the proposed ISS observer can accurately estimate battery SOC in real vehicle running circumstances, in which the charging-discharging current would change violently.

## V. Conclusion

This paper proposes a nonlinear state observer based on the ISS theory to estimate SOC of lithium-ion battery. We set up equivalent circuit model with two RC networks, considering the hysteresis characteristic when the lithium-ion battery is in charging and discharging process. And the hysteresis model parameters are identified by the measurement data acquired from a commercial lithium-ion battery on a test bench. Then the ISS based estimator has been set up to estimate SOC of the lithium-ion battery. Simulation results denote the ISS based estimator for the SOC estimation has high accuracy, and improved robustness. The designed observer is also tested on AMESim and Simulink co-simulation. The simulation results show that the state observer based ISS theory in this paper could trace the theoretical SOC well with the modeling error, and the estimation error is restricted in the required bound even when the model error or the initial SOC value is large.

In future work, the underlying battery model will be extended taking battery aging (capacity fade and resistance rise) into account.

## References

[1] L. G. Lu, X. B. Han, J. Q. Li, J. F. Hua, and M. G. Ouyang, "A review on the key issues for lithium-ion battery management in electric vehicles," *J. Power Sources*, vol. 226, pp. 272−288, Mar. 2013.

[2] J. Kim, G. S. Seo, C. Chun, B. H. Cho, and S. Lee, "OCV hysteresis effect-based SOC estimation in extended Kalman filter algorithm for a LiFeP$O_4$/C cell," in *Proc. IEEE Int. Electric Vehicle Conf.*, Greenville, SC, 2012, pp. 1−5.

[3] X. P. Chen, W. X. Shen, Z. W. Cao, and A. Kapoor, "A novel approach for state of charge estimation based on adaptive switching gain sliding mode observer in electric vehicles," *J. Power Sources*, vol. 246, pp. 667−678, Jan. 2014.

[4] S. Piller, M. Perrin, and A. Jossen, "Methods for state-of-charge determination and their applications," *J. Power Sources*, vol. 96, no. 1, pp. 113−120, Jun. 2001.
[5] J. B. Li, J. K. Barillas, C. Güenther, and M. A. Danzer, "A comparative study of state of charge estimation algorithms for LiFeP$O_4$ batteries used in electric vehicles," *J. Power Sources*, vol. 230, pp. 244−250, May 2013.
[6] J. K. Barillas, J. H. Li, C. Günther, and M. A. Danzer, "A comparative study and validation of state estimation algorithms for Li-ion batteries in battery management systems," *Appl. Energy*, vol. 155, pp. 455−462, Oct. 2015.
[7] W. He, N. Williard, C. C. Chen, and M. Pecht, "State of charge estimation for electric vehicle batteries using unscented Kalman filtering," *Microelectron. Reliab.*, vol. 53, no. 6, pp. 840−847, Jun. 2013.
[8] S. Sepasi, R. Ghorbani, and B. Y. Liaw, "A novel on-board state-of-charge estimation method for aged Li-ion batteries based on model adaptive extended Kalman filter," *J. Power Sources*, vol. 245, pp. 337−344, Jan. 2014.
[9] L. Zhong, C. B. Zhang, Y. He, and Z. H. Chen, "A method for the estimation of the battery pack state of charge based on in-pack cells uniformity analysis," *Appl. Energy*, vol. 113, pp. 558−564, Jan. 2014.
[10] F. L. Zhong, H. Li, S. M. Zhong, Q. S. Zhong, and C. Yin, "An SOC estimation approach based on adaptive sliding mode observer and fractional order equivalent circuit model for lithium-ion batteries," *Commun. Nonlinear Sci. Numer. Simul.*, vol. 24, no. 1−3, pp. 127−144, Jul. 2015.
[11] J. C. Álvarez Antón, P. J. García Nieto, F. J. de Cos Juez, F. Sánchez Lasheras, M. González Vega, and M. N. Roqueñí Gutiérrez, "Battery state-of-charge estimator using the SVM technique," *Appl. Math. Model.*, vol. 37, no. 9, pp. 6244−6253, May 2013.
[12] E. D. Sontag, "Smooth stabilization implies coprime factorization," *IEEE Trans. Auto. Control*, vol. 34, no. 4, pp. 435−443, Apr. 1989.
[13] S. Y. Wu, S. W. Mei, and X. M. Zhang, "Estimation of LISS (local input-to-state stability) properties for nonlinear systems," *Sci. China Technol. Sci.*, vol. 53, no. 4, pp. 909−917, Apr. 2010.
[14] Q. Zhu, J. R. Cui, and G. D. Hu, "Mean-square exponential input-to-state stability of numerical solutions for stochastic control systems," *Acta Automat. Sin.*, vol. 39, no. 8, pp. 1360−1365, Aug. 2013.
[15] B. Z. Gao, H. Chen, H. Y. Zhao, and K. Sanada, "A reduced-order nonlinear clutch pressure observer for automatic transmission," *IEEE Trans. Control Syst. Technol.*, vol. 18, no. 2, pp. 446−453, Mar. 2010.
[16] Y. F. Hu, C. Li, J. Li, H. Y. Guo, P. Y. Sun, and H. Chen, "Observer-based output feedback control of electronic throttles," *Acta Automat. Sin.*, vol. 37, no. 6, pp. 746−754, Jun. 2011. (in Chinese)
[17] G. S. M. Mousavi and M. Nikdel, "Various battery models for various simulation studies and applications," *Renew. Sustain. Energy Rev.*, vol. 32, pp. 477−485, Apr. 2014.
[18] C. Y. Xia and C. Zhang, "Real-time optimization control algorithm of energy management strategy for hybrid electric vehicles," *Acta Automat. Sin.*, vol. 41, no. 3, pp. 508−517, Mar. 2015. (in Chinese)
[19] M. García-Plaza, D. Serrano-Jiménez, J. Eloy-García Carrasco, and J. Alonso-Martínez, "A Ni-Cd battery model considering state of charge and hysteresis effects," *J. Power Sources*, vol. 275, pp. 595−604, Feb. 2015.
[20] G. L. Plett, "Extended Kalman filtering for battery management systems of LiPB-based HEV battery packs- Part 2. Modeling and identification," *J. Power Sources*, vol. 134, no. 2, pp. 262−276, Aug. 2004.
[21] M. Mastali, J. Vazquez-Arenas, R. Fraser, M. Fowler, S. Afshar, and M. Stevens, "Battery state of the charge estimation using Kalman filtering," *J. Power Sources*, vol. 239, pp. 294−307, Oct. 2013.
[22] M. A. Roscher and D. U. Sauer, "Dynamic electric behavior and open-circuit-voltage modeling of LiFeP$O_4$-based lithium-ion secondary batteries," *J. Power Sources*, vol. 196, no. 1, pp. 331−336, Jan. 2011.
[23] X. S. Hu, S. B. Li, and H. E. Peng, "A comparative study of equivalent circuit models for Li-ion batteries," *J. Power Sources*, vol. 198, pp. 359−367, Jan. 2012.
[24] M. Verbrugge and E. Tate, "Adaptive state of charge algorithm for nickel metal hydride batteries including hysteresis phenomena," *J. Power Sources*, vol. 126, no. 1−2, pp. 236−249, Feb. 2004.
[25] M. Kim, D. Jung, and K. Min, "Hybrid thermostat strategy for enhancing fuel economy of series hybrid intracity bus," *IEEE Trans. Veh. Technol.*, vol. 63, no. 8, pp. 3569−3579, Oct. 2014.
[26] D. H. Jeon, "Numerical modeling of lithium ion battery for predicting thermal behavior in a cylindrical cell," *Curr. Appl. Phys.*, vol. 14, no. 2, pp. 196−205, Feb. 2014.

**Yan Ma** received the B. S. degree in the Automation Department from Harbin Engineering University, China, in 1992, M. S. and Ph. D. degrees in the Department of Control Science and Engineering from Jilin University, China, in 1995 and 2006. In 1995, she joined former Jilin University of Technology. She has been a post doctor at Poly University, Hong Kong, China. Since 2009, she has been a professor at Jilin University. Her current research interests include nonlinear estimation methods and applications in power management system of EV, and robust filter methods.

**Bingsi Li** graduated from Jilin University, China, in 2014. She is currently a master student in the Department of Control Science and Engineering, Jilin University, China. Her main research interest is battery management system of EV.

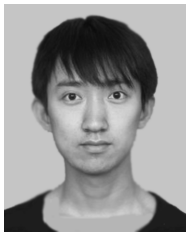

**Guangyuan Li** graduated from Jilin University, China, in 2015. He is currently a master student in the Department of Control Science and Engineering, Jilin University, China. His main research interest is battery management system.

**Jixing Zhang** received her M. S. degree from the Department of Control Science and Engineering, Jilin University, China, in 2015. Her main research interest is battery management system.

**Hong Chen** received the B. S. and M. S. degrees in process control from Zhejiang University, China, in 1983 and 1986, respectively, and Ph. D. degree from the University of Stuttgart, Germany, in 1997. In 1986, she joined Jilin University of Technology, China. From 1993 to 1997, she was a Wissenschaftlicher Mitarbeiter at the Institut Fuer Systemdynamik und Regelungstechnik, University of Stuttgart. Since 1999, she has been a professor at Jilin University, where she serves currently as Tang Aoqing Professor. Her current research interests include model predictive control, optimal and robust control, nonlinear control and applications in process engineering and mechatronic systems. Corresponding author of this paper.